OPEN

EPR-based Assessment of Gadolinium-based Contrast Agent Retention and Gadolinium Transchelation in Inflamed Murine Brain

Lina Anderhalten, MD, PhD, Nicole Höfer, MSc, Daria Dymnikova, MSc, Julia Hahndorf, MSc, Matthias Taupitz, MD, Heike Traub, PhD, Christian Teutloff, PhD, Carmen Infante-Duarte, PhD, and Robert Bittl, PhD

Objectives: In view of the mounting evidence for markedly increased cerebellar Gd retention under neuroinflammatory conditions after repeated linear GBCA administration *in vivo*, we aimed to discriminate between Gd retained within the GBCA complex and forms dissociated from the complex within the CNS and to characterize the chemical environment of the released Gd^{3+}. For this purpose, we used electron paramagnetic resonance (EPR) spectroscopy, which enables direct detection of Gd^{3+} release and evaluation of its molecular surroundings in intact cerebellar tissue from inflamed and noninflamed brain sections exposed to either linear or macrocyclic GBCAs.

Materials and Methods: We performed EPR and electron-nuclear double resonance (ENDOR) experiments on sub-mm brain samples taken after administration of linear gadopentetate-dimeglumine and macrocyclic gadobutrol *in vivo* in a murine multiple sclerosis model and *ex vivo* in organotypic hippocampal slice cultures under inflammatory conditions. Complementary mass spectrometry (MS) and MRI calibration experiments on Gd-spiked homogenized mouse brain tissue were used to identify potential Gd bindings and assess the relaxation-active fraction of retained Gd.

Results: EPR detected μM range Gd levels in intact cerebellar biopsies and slices and distinguished between complex-bound and released Gd following linear GBCA administration *in vivo*. In biopsies, we detected by ENDOR phosphorus-containing molecules in the microenvironment of released Gd. Binding to inorganic ligands was evidenced using MS and MRI calibration experiments in homogenized mouse brain tissue.

Conclusions: EPR and ENDOR proved to be sensitive methods for detecting Gd^{3+} release and characterizing retained Gd species within intact brain tissue. Our findings demonstrate inflammation-promoted Gd retention, underscore the importance of integrating *in vivo* and *ex vivo* analyses to unravel mechanisms of long-term Gd retention, and suggest that conventional MRI may underestimate the true extent of Gd accumulation, especially under neuroinflammatory conditions.

Key Words: electron paramagnetic resonance, experimental autoimmune encephalomyelitis, gadolinium-based contrast agents, gadolinium retention, laser ablation inductively coupled plasma mass spectrometry, magnetic resonance imaging, multiple sclerosis, neuroinflammation, organotypic hippocampal slice cultures, phosphate interaction

(*Invest Radiol* 2026;00:000–000)

Gadolinium (Gd) retention following the administration of gadolinium-based contrast agents (GBCAs) for magnetic resonance imaging (MRI) has obtained considerable scientific interest over the past decade. Repeated intravenous (IV) injections of GBCAs based on linear Gd complexes (linear GBCAs) appear to result in Gd retention in different human body tissues.[1,2] Since free ionic Gd (Gd^{3+}) is known to be highly cytotoxic, multiple studies were performed to investigate the mechanisms of Gd retention.[1] For the central nervous system (CNS), this phenomenon was reported for the first time in 2014 and showed that the cerebellar nuclei (CN) are sites prone to Gd retention.[3] Subsequent investigations, comprising numerous human[4–8] and animal studies,[9–14] have consistently validated sustained Gd retention within the brain *in vivo* after linear

Received for publication November 10, 2025; and accepted for publication, after revision, January 26, 2026.

From the Experimental and Clinical Research Center, A Cooperation Between the Max Delbrück Center for Molecular Medicine in the Helmholtz Association and Charité—Universitätsmedizin Berlin, Berlin, Germany (L.A., C.I.D.); Freie Universität Berlin, Fachbereich Physik, Berlin, Germany (N.H., D.D., C.T., R.B.); Department of Radiology, Charité—Universitätsmedizin Berlin, Corporate Member of Freie Universität Berlin and Humboldt-Universität zu Berlin, Berlin, Germany (J. H., M.T.); and Division Inorganic Trace Analysis, Bundesanstalt für Materialforschung und -prüfung (BAM), Berlin, Germany (H.T.).

L.A. and N.H.: equally contributing authors.

C.I.D., C.T., and R.B.: Conceptualization of the project; L.A.: performing *in vivo* mouse experiments and *ex vivo* hippocampal organotypic brain slice cultures; L.A., N.H., and D.D.: tissue processing and EPR sample preparation; N.H. and D.D.: performing EPR/ENDOR experiments; N.H., D.D., C.T., and R.B.: EPR data evaluation and analysis; L.A., J.H., and M.T.: sample preparation for MRI calibration, MRI acquisition and formal data analysis; L.A. and H.T.: LA-ICP-MS data acquisition and interpretation; L.A., N.H., and D.D.: data visualization; L.A., N.H., and D.D.: writing - original draft preparation; L.A., N.H., C.I.D., and R.B. with contributions from all coauthors: writing – editing and final manuscript; M.T., H.T., C.T., C.I.D., and R.B.: funding acquisition and supervision. All authors have read and agreed to the submitted version of the manuscript.

The original version of this manuscript was previously posted to arXiv: doi: http://arxiv.org/abs/2512.05615.

Conflicts of interest and sources of funding: We thank Bibiane Seeger-Schwinge for technical support during experimental mouse procedures, Susanne Müller for support in MRI (both at Charité), and Jessica Saatz (at BAM) for support in LA-ICP-MS. We gratefully acknowledge financial support from the Hertie Foundation to L. Anderhalten (medMS program) and funding by Deutsche Forschungsgemeinschaft (DFG) within the Collaborative Research Center (CRC) 1340, "Matrix in Vision" (projects A03, B03, B05, and C02), Grant No. 372486779.

Correspondence to: Carmen Infante-Duarte, PhD, Experimental and Clinical Research Center (ECRC), Charité–Universitätsmedizin Berlin, Campus Buch, Lindenberger Weg 80, 13125 Berlin, Germany. E-mail: carmen.infante@charite.de; Robert Bittl, PhD, Freie Universität Berlin, Fachbereich Physik, Arnimallee 14, 14195 Berlin, Germany. E-mail: robert.bittl@fu-berlin.de.

Supplemental Digital Content is available for this article. Direct URL citations are provided in the HTML and PDF versions of this article on the journal's website, www.investigativeradiology.com.

ISSN: 1536-0210
DOI: 10.1097/RLI.0000000000001280

GBCA administration. Contrary to that, cerebral accumulation associated with the administration of macrocyclic GBCAs was shown to be nonpermanent, characterized by a gradual, compound-specific washout occurring over weeks to months in animal models[15–19] and over months to years in humans.[20] As a result, the European Medicines Agency restricted the clinical utilization of linear GBCAs,[21] while the US Food and Drug Administration released class warnings and recommendations to limit their use.[22]

The probability of Gd deposition in brain tissue was reported to depend largely on the GBCA-specific kinetic inertness, which is higher for macrocyclic compared with linear GBCAs.[2,23,24] While macrocyclic Gd complexes are expect ed to be cleared from the brain as intact chelates,[25–28] linear Gd complexes may gradually dissociate *in vivo* and release Gd^{3+} from their chelating ligand when entering brain areas rich in competing endogenous ions such as copper (Cu),[29,30] zinc (Zn),[29–31] and iron (Fe).[29–32] Released Gd^{3+} may react with anionic inorganic phosphates and precipitate, forming long-lasting insoluble deposits of Gd phosphate salt ($GdPO_4$) within the CNS.[23,33] In addition, Gd^{3+} may also bind to endogenous molecules with complexing abilities,[11,25,27,34] like adenosine triphosphate (ATP).[35] Recent studies have identified potential Gd^{3+}-binding partners, such as ferritin,[33] citrate,[36] or glycosaminoglycan structures found in the extracellular matrix (ECM) or on cell surfaces.[34,36,37] However, the nature of these deposits remains unclear.

In patients with the chronic neuroinflammatory disease multiple sclerosis (MS), Gd retention in the brain was shown using MRI after multiple injections of linear GBCAs[4,38–42] and macrocyclic GBCAs,[43,44] yet the latter was subject to controversy.[45,46] Previous work using chronic and relapsing-remitting experimental autoimmune encephalomyelitis (EAE), a common mouse model of MS, demonstrated that brain inflammation can markedly increase cerebellar Gd retention levels after repeated IV injections of linear GBCA[47–49] and alter its spatial distribution patterns, even over extended periods.[48] In contrast, application of the macrocyclic GBCA gadobutrol led to a temporary retention of Gd that was efficiently cleared.[48] Thus, the EAE model is well suited to elucidate the causes of *in vivo* Gd^{3+} release and the mechanisms underlying sustained, potentially permanent Gd retention in the CNS, such as a proinflammatory milieu and/or endogenous destabilizing or transchelating tissue factors.

The quantification of Gd retention within CNS tissue following GBCA administration *in vivo* has been mainly conducted by techniques such as inductively coupled plasma mass spectrometry (ICP-MS) or laser ablation ICP-MS (LA-ICP-MS).[29,48,50–52] To be able to distinguish between intact GBCA, transchelated Gd^{3+}, and deposited Gd species, ICP-MS can be combined with chromatography techniques, which, however, require complex sample processing, potentially influencing the local Gd environment.[25,27,53,54]

Electron paramagnetic resonance (EPR) techniques have the potential for detection of Gd^{3+} release and the determination of its local molecular environment without sample manipulation.[55] However, while EPR is widely used in *in cell* studies, especially to explore protein conformations,[56,57] its utilization to study intact tissue samples is scarce.

In this study, we utilized EPR and electron-nuclear double resonance (ENDOR) spectroscopy to analyze Gd retention and its chemical environment in intact cerebellar biopsies of EAE and healthy control (HC) mice following repeated *in vivo* administration of GBCA. We applied the linear GBCA gadopentetate-dimeglumine or the macrocyclic GBCA gadobutrol as representatives for the 2 GBCA classes in line with previous work.[47,48,58] To assess the stability of Gd retention and the Gd environment, we also conducted EPR measurements on homogenates of chronic organotypic hippocampal slice cultures exposed to GBCA *ex vivo* under inflammatory conditions.

Magnetic resonance-based techniques like *in vivo* MRI and EPR may be limited in their ability to detect inorganic precipitated forms of Gd and previous studies have reported discrepancies between MRI-derived Gd detection and elemental quantification by (LA-)ICP-MS.[48,50,52,59] Therefore, we additionally performed an MRI *in vitro* calibration to determine the relaxation active amount of retained Gd and thereby estimate inorganic Gd bindings.

MATERIALS AND METHODS

Animal Ethics

Mouse experiments were performed in accordance with the European Communities Council Directive of 22 September 2010 (2010/63/EU). All experimental procedures were approved by the Berlin State Office for Health and Social Affairs (LAGeSo; approval IDs: G106/19, TCH0008/20).

Mouse Model of EAE and *In Vivo* Administration of GBCAs

The EAE and control animal tissues used in this study originate from animals included in our previous study reported in Anderhalten et al 2022.[48] That study comprised longitudinal *in vivo* MRI and LA-ICP-MS analyses following repeated administration of gadopentetate or gadobutrol in EAE or HC mice. The present work builds on this cohort and focuses on EPR-based analyses performed in a defined subset of animals, as detailed below.

EAE was actively induced in 10-week-old female SJL/J mice (Janvier Labs, France) by subcutaneous immunization with proteolipid protein peptide ($PLP_{139\text{-}151}$; purity 95%; Pepceuticals, Leicester, United Kingdom).[47,48] Starting at the peak of disability (day 12 post-immunization), EAE mice were exposed to repeated IV injections of either a linear GBCA ($n = 1$; gadopentetate dimeglumine, Magnevist, 0.5 mmol/mL, Bayer, Germany), hereafter referred to as gadopentetate, or macrocyclic GBCA ($n = 1$; gadobutrol, Gadovist, 1.0 mmol/mL, Bayer, Germany) at a cumulative dose of 20 mmol/kg body weight (BW). As illustrated in Figure 1A, 4 consecutive daily GBCA injections were followed by a 2-day break and 4 additional injections (overall 8×2.5 mmol/kg BW), as previously described.[47,48] In addition, HC mice received either gadobutrol or gadopentetate, respectively, following the same injection regimen.

For the purposes of the present EPR-focused study, brain tissue material from one GBCA-treated mouse per group (HC gadopentetate, EAE gadopentetate, HC gadobutrol, and EAE gadobutrol, as previously characterized) was selected. The mice were sacrificed 10 days after the final GBCA administration with an overdose of ketamine/xylazine (50 mg/mL ketamine, 20 mg/mL xylazine, in 0.9% NaCl). An untreated HC mouse of the same strain, age, and sex was used as a negative control (Fig. 1A). Mouse bodies were transcardially perfused with 50 mL of 0.1 M PBS (Ismatec ISM444B-115 V Analog Peristaltic Pump). Subsequently, brains were extracted and fixed in 4% paraformaldehyde (PFA) and 30% sucrose. Thereafter, they were coronally separated into the forebrain, midbrain, and cerebellum and stored at −80°C. Brain tissue from these animals was processed for EPR measurements, as illustrated in Figure 1A.

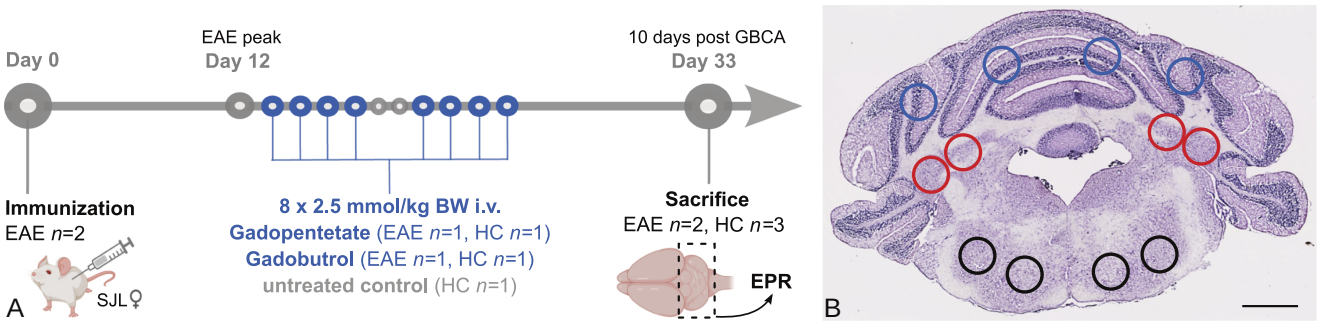

FIGURE 1. A, Experimental mouse setup for EPR sampling with repeated *in vivo* injections of either gadopentetate or gadobutrol in EAE mice ($n = 2$) or HC mice ($n = 2$) at 2.5 mmol/kg BW each (8 daily injections from day 13 to 23 with a 2-day pause in between; cumulative dose of 20 mmol/kg BW). These GBCA-treated mice (n = 4) and one untreated HC mouse as negative control were sacrificed 10 days post-GBCA administration and brains were processed for EPR measurements. This EPR-focused experimental design represents a simplified subset of the *in vivo* study previously described,[48] from which the animals and tissue samples were derived. B, Exemplary visualization of the location of brain biopsies for EPR measurements in a cerebellar hematoxylin and eosin-stained EAE mouse brain section at 2× magnification. Blue outlines indicate the position of biopsies from the cerebellar cortex, red outlines indicate CN, and black outlines indicate the medulla. (Scale bar 1 mm).

Collection of Biopsies From Mouse Cerebellum

Cerebellar tissue from EAE ($n = 2$) and HC mice ($n = 2$) treated with gadopentetate or gadobutrol, and from an untreated HC mouse ($n = 1$, negative control) was used for the evaluation of Gd retention and possible Gd complex dissociation *in vivo* using EPR. Mouse cerebella were thawed at room temperature, washed in 1 M sodium chloride, and transferred to a clean glass slide with the caudal part facing down. Three distinct brain regions were biopsied from each cerebellum, resulting in a total of 3 biopsy samples per mouse brain. The cerebellar regions of interest (ROI) were chosen based on our recently published data on Gd retention patterns in EAE brains using LA-ICP-MS.[48] As displayed in Figure 1B, biopsies were collected from (i) the cerebellar cortex, (ii) the CN, and (iii) the medulla using quartz capillaries for EPR (Vitrocom, Mountain Lakes, USA) with 0.87 mm/0.7 mm outer/inner diameters (OD/ID) (see also Fig. S1, Supplemental Digital Content 1, http://links.lww.com/RLI/B103). To obtain sufficient tissue material in the EPR capillaries, each brain ROI was sampled 4 times (Fig. 1B). Biopsy-containing capillaries were then centrifuged at 100 to 200 g for 2 min (Eppendorf Centrifuge 5417c, Eppendorf AG, Germany) to ensure that the tissue was positioned at the closed bottom of the capillaries for subsequent EPR measurements.

Generation of Organotypic Hippocampal Tissue Slice Cultures

Chronic organotypic brain slices of the hippocampus were generated following an established protocol.[58] Briefly, 7- to 10-day-old pups of the B6.Cg-Tg(Thy1-CFP/COX8A) S2Lich/J strain (FEM animal facility, Berlin Buch, Germany) were sacrificed by decapitation. The scalp was removed and the skull was placed on chilled cutting medium (1× MEM with 1% L-Glutamine). Under sterile conditions, the skull was opened, and the hippocampi were isolated and sliced into 350 µm-thick sections using a McIlwain Tissue Chopper (Mickle Laboratory Engineering Co., Ltd., Guildford, Surrey, UK). Intact slices were placed onto polytetrafluoroethylene (PTFE) membrane culture inserts (PICM0RG50, Millicell cell culture inserts, 0.4 µm) in 6-well plates in a randomized manner (6 to 8 slices per membrane, 3 replicate membranes per culture condition). Slices were cultured at 37°C and 5% CO_2 using a modified culture medium based on the study by Wang et al[60] [1× MEM, 25% HBSS, 25% heat-inactivated horse serum, 13 mM HEPES, Pen/Strep (ingredients from Gibco™, Thermo Fisher Scientific Inc., Waltham, MA, USA), and 35 mM glucose (B. Braun, Melsungen, Germany)], which was changed every second day.

Chronic Tissue Slice Culture Treatment With GBCAs *Ex Vivo*

After 13 days in culture, slices were exposed to either gadopentetate or gadobutrol at 1 mM for 48 h, in line with our previous study[48] and as illustrated in Figure 2. To mimic an inflammatory milieu, hippocampal slices were additionally exposed to tumor necrosis factor α (TNFα; mouse recombinant, lyophilized; Invitrogen) at 50 ng/mL. Slices treated with TNFα without GBCA served as negative controls. For optimal substance penetration into the hippocampal tissue, 100 µL of the respective substance-enriched medium was applied on top of the membranes with the slices [3 conditions: (1) TNFα; (2) 1 mM gadopentetate + TNFα; (3) 1 mM gadobutrol + TNFα]. On day 15, to stop treatment, the membranes were washed repeatedly with fresh prewarmed culture medium (3×10 min at 37°C, 5% CO_2; Fig. 2). To ensure a precise 48 h incubation per condition, treatment initiation on day 13 was time-staggered to match termination 48 h later on day 15. Thereafter, slices were incubated for one more week without additives; culture medium was changed every 2 days (Fig. 2).

Processing of Chronic Organotypic Hippocampal Tissue Slice Cultures

On day 23, membranes were cut out from the respective cell culture inserts with a sterile scalpel ($n = 3$ per condition) and transferred into a 2 mL Eppendorf tube containing 0.5 mL of fresh culture medium. Using a mechanical homogenizer with a sterile pestle (Argos Technologies, Inc., Illinois, USA), the tube content was homogenized for 2 min to detach tissue samples from the PTFE membranes. Membranes were discarded, the tubes centrifuged for 2 min (400 g, Eppendorf Centrifuge 5417R, Eppendorf AG, Germany), and the supernatant was removed. The remaining tissue pellet was further washed with fresh culture medium in 2 more rounds of homogenization and centrifugation to remove unbound GBCA from the tissue sample. In the last step, the tissue pellet was homogenized with 20 µL medium for 30 seconds. The described process was repeated for each culture condition. As shown in Figure 2, the

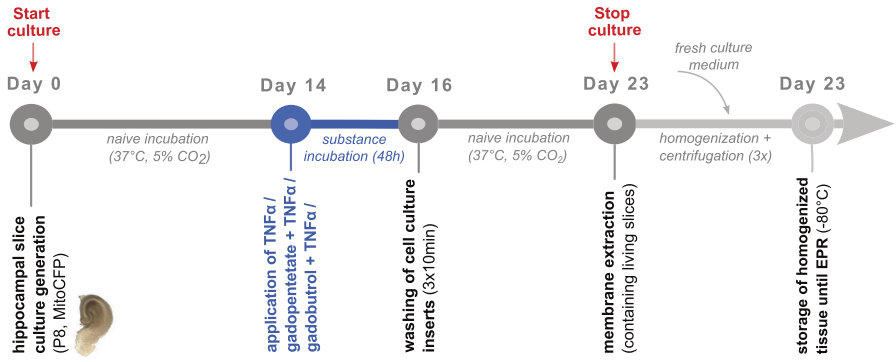

FIGURE 2. Illustration of the experimental *ex vivo* setup. Chronic organotypic hippocampal cultures were exposed for 48 h to GBCAs and TNFα starting on day 14 post-preparation [3 conditions: (1) TNFα at 50 ng/mL, (2) 1 mM gadopentetate + TNFα, (3) 1 mM gadobutrol + TNFα]. On day 16, slices were washed several times and cultured for an additional week without substances. On day 23, culture membranes containing hippocampal slices were carefully extracted. After repeated homogenization and centrifugation steps with fresh culture medium (3 times, 0.5 mL medium each), one final tissue homogenate per condition was obtained.

resulting tissue homogenates were stored at –80°C before they were thawed and filled into quartz capillaries (Vitrocom, Mountain Lakes, USA) with 0.87 mm/0.7 mm OD/ID, centrifuged, and frozen for EPR assessment.

EPR/ENDOR

EPR measurements were performed on pure gadopentetate and gadobutrol, on the brain biopsy samples from the *in vivo* mouse experiment [5 conditions: (1) untreated HC mouse (= negative control), (2) gadopentetate-treated EAE, (3) gadobutrol-treated EAE, (4) gadopentetate-treated HC, (5) gadobutrol-treated HC], on the tissue homogenates of the chronic hippocampal slice cultures referred to as "*slices*" [3 conditions: (1) TNFα (= negative control), (2) 1 mM gadopentetate + TNFα, (3) 1 mM gadobutrol + TNFα], and on the reference samples Gd-ATP, gadopentetate-ATP, gadobutrol-ATP, Gd-DMPC, and $GdCl_3$ in aqueous solution. For the measurements, the highest microwave frequency available, W-band (94 GHz), was used due to the high sensitivity (~1 μM) and small sample volumes required (~1 μL). Details of the reference samples and their preparation are given in the Supplementary Digital Content 1, http://links.lww.com/RLI/B103.

Continuous wave (cw) EPR and pulsed ENDOR were performed on a Bruker Elexsys E680 W-band (94 GHz) EPR spectrometer using a Bruker Teraflex EN600-1021H probe head. For ENDOR experiments, a Bruker DICE-II unit operating in stochastic mode and a radiofrequency (RF) amplifier AR-150A400 (Amplifier Research, Souderton, USA) were additionally used.

Besides higher sensitivity compared with conventional 9 GHz (X-band) EPR, W-band EPR offers the additional advantage that the spectra of systems with high electron spin *S*, like Gd^{3+} ($S = 7/2$) are strongly dominated by the rather narrow central transition ($m_S = -1/2 \leftrightarrow m_S = +1/2$) with only weak contributions from the much broader higher m_S transitions.[61]

All cw EPR spectra were recorded with lock-in detection (100 kHz field modulation frequency with an amplitude of 0.5 mT and a conversion time of 60 ms), 80 μT field steps, and at a temperature of 80 K. As usual, the cw EPR spectra are presented as the first derivative, those from pulsed experiments as absorption spectra. Details of the used pulse ENDOR sequences[62,63] are also given in the Supplementary Digital Content 1, http://links.lww.com/RLI/B103. All ENDOR spectra were recorded at a temperature of 10 K.

Analysis of EPR and ENDOR Spectra

All cw EPR spectra were analyzed and plotted using Matlab version 9.14.[64] A linear background was subtracted, and all spectra were normalized separately for the biopsies and tissue slices after GBCA treatment. In each group the spectra were normalized to the sample with the largest peak-to-peak amplitude of the third Mn^{2+} line on the low-field side. Then, the spectrum of the respective control sample without GBCA treatment was subtracted, scaled individually to minimize the Mn^{2+} signal in each difference spectrum (see Supplemental Digital Content 1, Fig. S2, http://links.lww.com/RLI/B103, which visualizes a cw EPR difference spectrum). The normalization on Mn^{2+} is justified, as previous cerebellar LA-ICP-MS data on Mn showed a relatively homogeneous distribution of Mn across the different brain sections studied, eliminating the uncertainty in the sample amount due to inconsistent filling of the EPR capillary. These reference Mn data were obtained in the context of our previous study but were not included in Anderhalten et al.[48] A lower limit for the concentration of retained Gd can then be achieved under the assumption of an optimum filling of the capillary with the largest Mn^{2+} signal by comparing the signal intensity of interest in the difference spectrum with the GBCA reference spectrum.

To facilitate the identification of the peak positions in the ENDOR spectra, the ^{1}H ENDOR spectrum of the gadopentetate-treated EAE mouse biopsy, as well as the ^{31}P ENDOR spectrum of the Gd-DMPC reference spectrum, was symmetrized around the central frequency. Spectra of low signal-to-noise ratio were smoothed by using a binomially weighted moving average taken over a window of maximally 5 (cw EPR), 11 (^{1}H ENDOR), and 17 (^{31}P ENDOR) points. Gd-P distances were extracted by fitting the ENDOR spectra using the *saffron* and *esfit* functions of the EasySpin package.[65] Details on the P ENDOR analysis are given in the Supplemental Digital Content 2 (Fig. S5), http://links.lww.com/RLI/B104.

MRI Calibration in Homogenized Mouse Tissue

Determination of local Gd concentrations in tissue by *in vivo* T_1-mapping is hampered by the fact that the paramagnetic efficacy (^{1}H NMR T_1 relaxivity (r_1))[66] of Gd depends on various factors, mainly the molecular tumbling rate/molecular weight of the Gd-containing molecule, chemical environment, temperature, viscosity, and others.[36,67] Vendor-provided nominal r_1 of the GBCA cannot be applied directly. The comparison of Gd

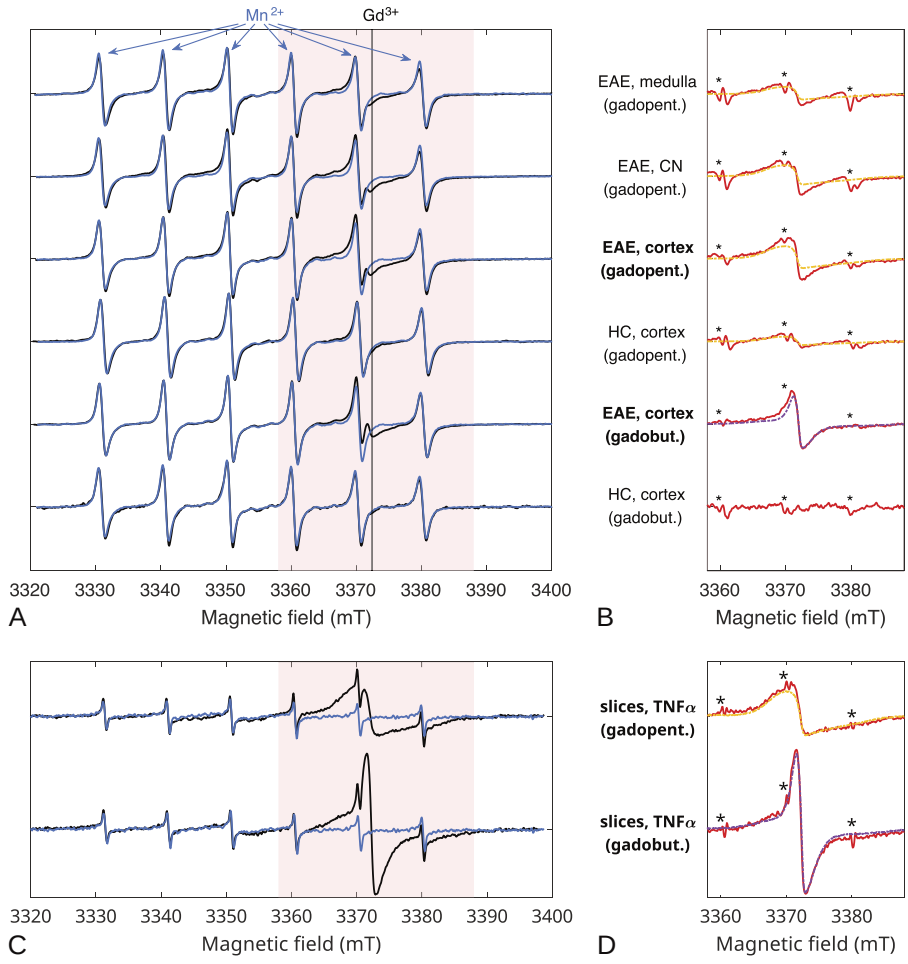

FIGURE 3. Comparison of cw EPR spectra. (A) Experimental cw EPR spectra (in black) of biopsies from different brain regions (medulla, CN, and/or exclusively cerebellar cortex) obtained from EAE and HC mice treated with either gadopentetate (linear GBCA) or gadobutrol (macrocyclic) are compared with normalized control sample spectra (in blue). The area highlighted in red corresponds to the field range evaluated in (B). There, differences between the blue and black spectra (all scaled by a factor of 2 compared with (A) are plotted in red and compared with the scaled corresponding pure GBCA spectra (gadopentetate: yellow, gadobutrol: purple). Residual Mn^{2+} artifacts are marked with asterisks. (C) Experimental cw EPR spectra of chronic slices incubated with gadopentetate or gadobutrol *ex vivo*, respectively, are compared with a negative control spectrum, along with (D) corresponding difference spectra compared with pure GBCA spectra. The 4 samples indicated in bold font were additionally measured with ENDOR.

concentrations from *in vivo* T_1-mapping and other quantitative analytical methods requires knowledge about the concentration-dependent r_1 of the GBCA in the tissue under the specific MRI conditions.

Therefore, an *in vitro* MRI calibration was conducted using brain tissue from eighteen 10-week-old female healthy SJL/J mice. Brains were isolated, flash-frozen in liquid nitrogen, and preserved at –80°C. Thereafter, the brains were cryopulverized using the CP02 cryoPREP Automated Dry Pulverizer (Covaris Ltd, UK) and manually homogenized with 5% fetal bovine serum (FBS). To obtain GBCA standards ranging from 20 to 100 μM (in 20 μM steps), either gadopentetate or gadobutrol was added to the homogenate at varying concentrations.[11] For baseline acquisition, samples without GBCA were prepared. Samples were transferred into 5 mm glass tubes and incubated for 30 minutes at 4°C. Subsequently, the tubes were warmed up to 37°C and MRI scans were performed on a 7 T small-animal scanner (Bruker BioSpec, Ettlingen, Germany), running ParaVision 6.1 software. An axial 2-dimensional T_1 map RARE-VTR sequence in analogy to[48] was used (echo time = 9.83 ms, 8 TRs from 255 to 7000 ms, rare factor = 2, field of view = 26 mm^2, matrix = 128×128, number of slices = 3, slice thickness: 1 mm, scan time: 17 min and 13 s). For internal validation, *in vitro* MRI calibration was also performed in water and pure FBS following the same protocol[37] (see Table S2, Supplemental Digital Content 3, http://links.lww.com/RLI/B105).

Subsequently, we compared the calibrated T_1 values to *in vivo* T_1 ($T_{1,iv}$; n = 8 to 10 per group) and LA-ICP-MS data (n = 2/group) 10 days post-GBCA administration from previously performed *in vivo* experiments[48] using the GBCA injection regimen in mice described in subsection "Mouse Model of EAE and *In Vivo* Administration of GBCAs", computing the percentage T_1 deviation of *in vivo* $T_{1,iv}$ from calculated $T_{1,c}$ ($= 1/R_{1,c}(C_{Gd})$; n = 2/group). Negative T_1 deviation corresponds to longer T_1 relaxation times than expected for the

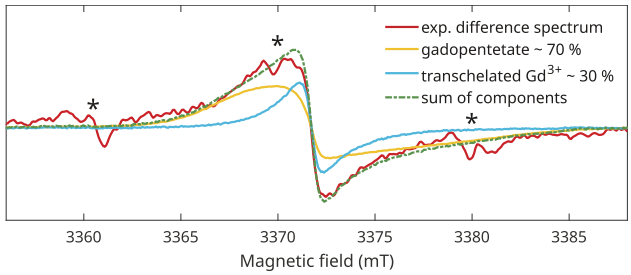

FIGURE 4. Decomposition of the difference spectrum (red) of the cortex biopsy from the EAE mouse treated with gadopentetate from Figure 3B (3rd spectrum) into a spectrum of pure gadopentetate (yellow) and of transchelated Gd^{3+} (cyan), represented by the spectrum of the $GdCl_3$ reference sample. The dashed green trace is the sum of the yellow and the cyan spectra. Residuals from the Mn^{2+} contribution are marked with asterisks.

Gd concentration. A detailed description of the experimental procedures and analyses is provided in Supplemental Digital Content 3, http://links.lww.com/RLI/B105.

LA-ICP-MS

For the LA-ICP-MS measurements, an NWR-213 laser ablation system equipped with a 2-volume sample chamber (Elemental Scientific Lasers, Bozeman, MT, USA) was coupled to an ICP sector-field mass spectrometer (Element XR; Thermo Fisher Scientific, Bremen, Germany). Cerebellar cryosections (thickness 10 μm) of EAE and HC mice (n = 2/experimental group) mounted on microscopic glass slide (SuperFrost Plus adhesion slides, Thermo Fisher Scientific, Schwerte, Germany) were ablated in an imaging mode. For the Gd quantification, agarose gels spiked with different Gd concentrations were used. Further details are given in Anderhalten et al.[48]

Data visualization was done in Origin 2018 (OriginLab Corporation, Northampton, MA, USA). The measured values for the isotopes ^{158}Gd and ^{55}Mn were used for the evaluation. Since the samples and the calibration standards based on spiked agarose have a natural isotope abundance, the Gd and Mn images reflect the quantitative distribution of Gd and Mn, respectively, (in μM) in the thin tissue sections.

To determine the Gd retention in certain brain areas (medulla, cerebellar cortex, and CN), manual ROIs were applied to the calibrated LA-ICP-MS images for Gd. The analysis of each ROI was conducted 3 times in an independent randomized manner using ImageJ (National Institute of Health, USA) for better reliability. Gd concentrations determined for the medulla, cerebellar cortex, and CN of EAE and HC mice 10 days after GBCA injection were averaged.

Statistics

The study data were statistically analyzed using R software (RStudio, version 2022.07.2). LA-ICP-MS and MRI calibration data were expressed descriptively ($n = 1$ to 2/group or condition, each) as geometric means ± SD. Concentration results obtained by cw EPR were given descriptively as total numbers, and results derived from ^{31}P ENDOR fits were stated as value ± SD or ± a resolution limit if the uncertainty provided by the fit was unreasonable (see Supplemental Digital Content 2, http://links.lww.com/RLI/B104). *In vivo* MRI data for the 3 brain biopsy regions ($n = 8$-10/group) were analyzed by applying nonparametric Mann-Whitney *U* tests for 2-group comparison, followed by Bonferroni correction for multiple testing (see Supplemental Digital Content 3, http://links.lww.com/RLI/B105). *P* values < 0.05 indicated statistical significance with * implying $P < 0.05$, ** implying $P < 0.01$, and *** implying $P < 0.001$.

RESULTS

Gd Retention in Brain Tissue After *In Vivo* and *Ex Vivo* Administration of GBCA

To assess the presence of Gd retention and to evaluate the potential release of Gd^{3+} from the GBCA complex, we recorded continuous wave (cw) EPR spectra of pure standards, the biopsies obtained 10 days after multiple IV injections of GBCAs (Figs. 3A, B), and the slices following 48 h-GBCA treatment *ex vivo* (Figs. 3C, D). Figures 3A and C depict the experimental spectra of GBCA-treated samples (black) in comparison to the respective negative control samples (blue). The spectra are dominated by 6 lines, which are due to traces of Mn^{2+} typically present in cell and tissue samples, and was also detected by LA-ICP-MS in the tissue thin sections of the mouse brains.[48] A broader (in part barely visible) feature on the high-field side of the fifth Mn^{2+} line (from the left) represents the Gd^{3+} signal. Figure 3B and D contain difference spectra (see Supplementary Digital Content 1, Fig. S2, http://links.lww.com/RLI/B103) between the GBCA-treated biopsy or slice samples of Figures 3A and C and their respective negative controls. The subtraction removed most of the Mn^{2+} signal, but left residuals around the Mn^{2+} line positions (marked with asterisks). The difference spectra (red) are displayed together with correspondingly scaled pure GBCA reference spectra (gadopentetate: yellow, gadobutrol: purple; also see Fig. S4, Supplemental Digital Content 1, http://links.lww.com/RLI/B103).

We detected similar amounts of retained Gd in the range of 2 to 3 μM for both GBCAs in the biopsies from different EAE cerebellar regions (cerebellar cortex, CN, and medulla), and about 1 μM in the cortex of the gadopentetate-treated HC mouse. The difference spectra (red) in Figure 3B of biopsies from the EAE mouse treated with the linear GBCA gadopentetate differ clearly from the pure GBCA spectrum (yellow). These 3 spectra can be deconvoluted into 2 contributions, as shown in Figure 4 for the cerebellar cortex sample. The main contribution is the spectrum of gadopentetate (yellow line) with a relative weight of 70%. The residual after subtraction of the gadopentetate contribution is a much narrower spectrum. A clear assignment of this second component is impossible since Gd^{3+} shows very similar cw EPR spectra in rather different environments, for example, in aqueous solution or in gadobutrol (see Supplementary Digital Content 1, Fig. S3, http://links.lww.com/RLI/B103). Within the limited signal-to-noise ratio (SNR) of the experimental spectrum, this second contribution can be represented by either of the two. The relative weight of this contribution is 30% and represents a Gd^{3+} proportion in an environment clearly distinct from the gadopentetate complex, that is, released/transchelated Gd. The Gd intensity measured on the cortical biopsy of the gadopentetate-treated HC mouse was close to the detection limit and a deconvolution was not attempted due to the low SNR of the spectrum.

The cortical biopsy of the EAE mouse treated with the macrocyclic GBCA gadobutrol shows a spectrum similar to the pure gadobutrol spectrum. Since the cw EPR spectrum of gadobutrol is much less distinct from the spectrum of the Gd^{3+} in aqueous solution than the spectrum of gadopentetate, deconvolution is not possible in this case, and no information on release/transchelation can be derived. It should further be noted that the larger signal amplitude of the EAE cortex biopsy

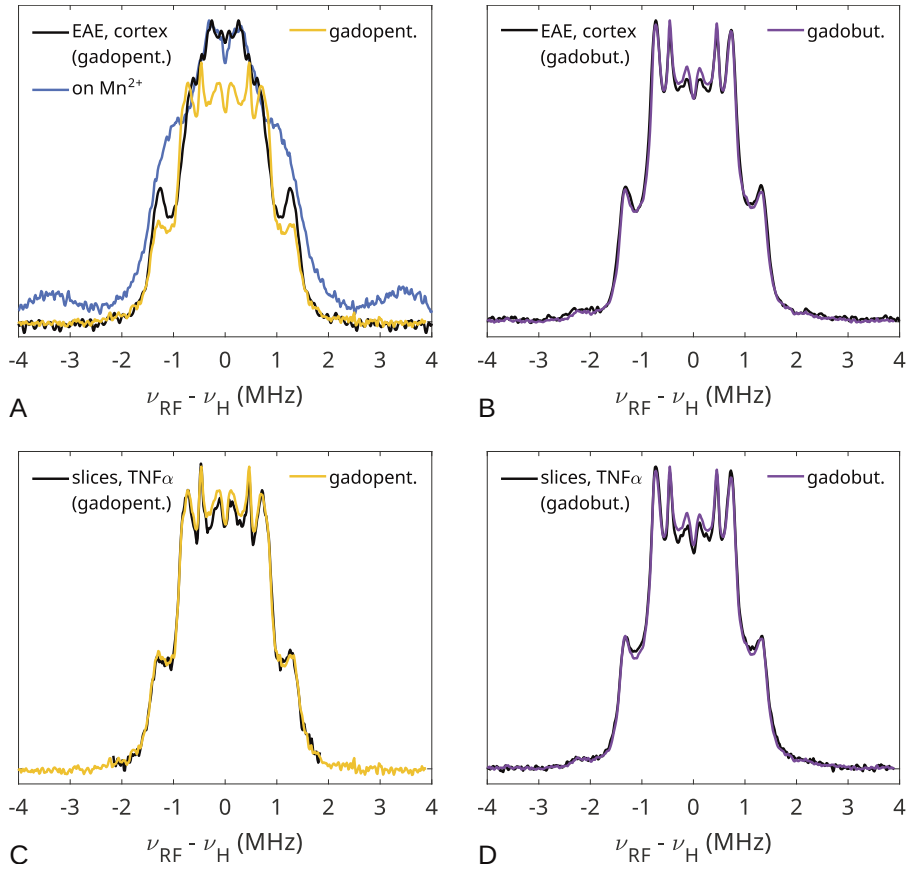

FIGURE 5. ^{1}H ENDOR spectra recorded on (A), (B) cortical mouse brain biopsies (black) and (C), (D) slices incubated with GBCA *ex vivo* (black), compared with the normalized spectra of the corresponding pure GBCA (gadopentetate: yellow, gadobutrol:purple). In (A), the spectrum for the Mn^{2+}-H couplings is shown in blue, recorded on the lowest-field Mn^{2+} line, where the Gd signal is negligible. In (A), the spectrum of pure gadopentetate was scaled for comparison; all other spectra were normalized to their maximum.

post-gadobutrol compared with post-gadopentetate is misleading in terms of Gd concentration due to the significantly lower line width and both samples contain similar Gd concentrations. The cortical biopsy of the gadobutrol-treated HC mouse did not show any Gd signal (Fig. 3B).

The Gd spectra obtained from slices incubated with GBCAs *ex vivo* (Fig. 3C) are indistinguishable from the spectra of the respective pure GBCA (Fig. 3D). Their intensities are up to 4-fold the signals of the Gd in the biopsies, corresponding to ~8 to 10 μM.

Environment of Retained Gd After *In Vivo* GBCA Administration

To further elucidate whether the retained Gd found in the different samples after GBCA administration was still bound within the parent GBCA complex, as well as to gain deeper insights into retention mechanisms and potential competing Gd binding sites within the tissues, we directly measured the local chemical environment of Gd using electron-nuclear double resonance (ENDOR). The ^{1}H ENDOR spectra of the cortical biopsies and slice samples are shown in Figure 5 (in black) in comparison to the spectra of the pure GBCAs (in yellow). The spectrum shown in blue in Figure 5A was recorded on the Mn^{2+} EPR signal part and represents Mn^{2+}-H hyperfine couplings. The absence of any significant intensity around ±3.5 MHz in the spectrum of the gadopentetate biopsy sample (Fig. 5A, black) recorded on the Gd^{3+} EPR signal shows the achieved efficient Mn^{2+} suppression. Thus, all spectra depicted in black correspond exclusively to Gd^{3+}-H hyperfine couplings.

The spectrum of the Gd couplings of the sample from the gadopentetate-treated EAE mouse clearly differs from the one of pure gadopentetate. In contrast, the spectra recorded for the gadobutrol-treated EAE mouse (Fig. 5B) as well as for the *ex vivo* slices treated with both gadopentetate (Fig. 5C) and gadobutrol (Fig. 5D) coincide with the spectra of the corresponding pure GBCA. The small differences in the center of the obtained spectra (below ±0.4 MHz), which correspond to very weak couplings and, therefore, large distances (Figs. 5B, C, D), can be neglected here. The pronounced spectral difference in the case of the gadopentetate-treated EAE mouse (Fig. 5A) demonstrates that at least a fraction of the retained Gd exists in an environment different from the GBCA complex cage.

Phosphorus in the Vicinity of Retained Gd

Since phosphorus occurs with 100% natural abundance as the ^{31}P magnetic isotope, it is an interesting species to probe in the vicinity of the retained Gd by ENDOR, even though Gd in the inorganic, solid $GdPO_4$ is invisible to EPR methods. Multiple organic phosphate-containing species, for example, organic phosphates in nucleotides, phospholipids, or proteins/sugars

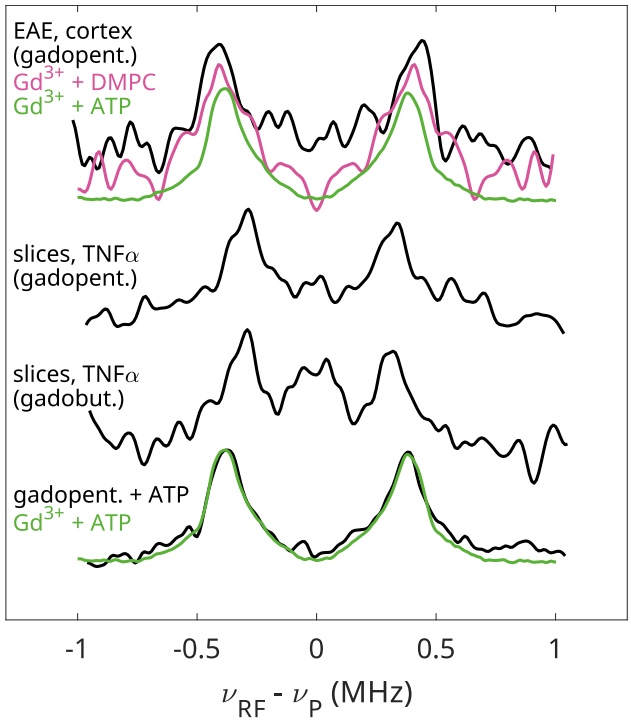

FIGURE 6. P ENDOR spectra recorded on the cortical mouse brain biopsy of the gadopentetate-treated EAE mouse and the slices incubated *ex vivo* (black; 3 upper plots). As references, the spectra of Gd-ATP (green), Gd-DMPC (magenta, symmetrized data), and gadopentetate-ATP are shown. Gd-DMPC and Gd-ATP are slightly shifted downwards compared with the biopsy spectrum (top) for clarity. All spectra are normalized to the maximum of the smoothed data. The spectra of the gadopentetate-treated EAE mouse and slices were measured with Mn suppression, the gadobutrol-treated slices as well as all the reference samples were measured with the standard sequence.

with phosphorylated residues are potential binding sites. The P ENDOR spectra of the cortical biopsy from the gadopentetate-treated EAE mouse and of the *ex vivo* slices treated with both GBCA are shown in Figure 6. The spectrum of the cortical biopsy (black, first plot) reveals distinct peaks at about ±0.4 MHz indicative for phosphate in the first coordination shell of Gd. Phosphate in the vicinity of Gd^{3+} was also detected in the GBCA-treated *ex vivo* slices for both GBCA. Additional ^{31}P Mims ENDOR were recorded for the reference samples Gd-ATP (green), Gd-DMPC (magenta), and gadopentetate-ATP (black). The spectra of the control samples of Gd-ATP (green) and gadopentetate-ATP (black) shown at the bottom are indistinguishable except for the much worse SNR for the gadopentetate-ATP sample at equal Gd concentrations.

The splitting between the peaks shown in Figure 6 encodes the hyperfine coupling between the Gd electron spin and the ^{31}P nuclear spin and provides a measure for the Gd-P distance. This splitting appears slightly larger for the EAE biopsy compared with the Gd-ATP reference sample (green) and seems to be in better agreement with the Gd-DMPC reference sample (magenta), which shows the largest peak splitting of the reference samples, that is, the shortest Gd-P distance. The slightly larger peak splitting for the EAE biopsy indicates a slightly shorter Gd-P distance than in Gd-ATP. The peak splittings are smaller for the slice samples than for Gd-ATP, indicating a larger Gd-P distance in these cases.

We extracted the ^{31}P hyperfine couplings and the respective Gd-P distances $r_{Gd\text{-}P}$ by least-square fitting (see Table S1, Supplemental Digital Content 2, http://links.lww.com/RLI/B104 for full P ENDOR fit results). The Gd-P distance obtained for the Gd-ATP reference is $r_{Gd\text{-}P} = 0.36 \pm 0.01$ nm, for the gadopentetate-treated EAE mouse sample $r_{Gd\text{-}P} = 0.35 \pm 0.01$ nm, for the *ex vivo* slice samples $r_{Gd\text{-}P} = 0.37 \pm 0.01$ nm, and for the Gd-DMPC reference $r_{Gd\text{-}P} = 0.36 \pm 0.03$ nm due to the low SNR.

The $r_{Gd\text{-}P}$ determined for Gd-ATP here is slightly larger than the $r_{Gd\text{-}P} = 0.35$ nm obtained from NMR relaxation,[35] however, it agrees with recent ENDOR data.[68] Furthermore, the Mn-P distance for Mn-ATP was significantly shorter[35] than the distance deduced from ENDOR.[69] A P ENDOR signal was measurable neither for the cortical biopsy sample of the gadobutrol-treated EAE mouse nor for a gadobutrol-ATP reference sample.

Interaction of Gd With Inorganic Ligands

We performed an *in vitro* MRI calibration experiment to reveal the relaxation active amount of bound and unbound Gd retained in the tissue. The relaxivity r_1 of gadopentetate and gadobutrol was computed using *in vitro* T_1 relaxometry, with standards containing ascending Gd^{3+} concentrations in water, FBS, and homogenized brain tissue (see Table S2, Supplemental Digital Content 3, http://links.lww.com/RLI/B105 for detailed results). Tested standards demonstrated a good fit to the linear regression model with relaxivities r_1(gadopentetate) = 4.35 $s^{-1}mM^{-1}$ and r_1(gadobutrol) = 6.96 $s^{-1}mM^{-1}$ (homogenized brain; gadopentetate, $R^2 = 0.97$; gadobutrol, $R^2 = 0.98$).

The computation of T_1 deviation (%) comparing *in vivo* T_1 values in the brain to calibrated T_1 values in brain homogenate at the respective Gd concentrations detected by LA-ICP-MS was performed for the 3 biopsy regions medulla, cerebellar cortex, and CN of EAE and HC mice (Fig. 7). The *in vivo* T_1 relaxometry and LA-ICP-MS data underlying our following results are reported here as part of the Supplemental Digital Content 3 (Fig. S6g-i and Table S3, http://links.lww.com/RLI/B105), with only the CN Gd concentrations having been previously published.[48] For better traceability of the T_1 deviation computation, here, the CN data at day 10 post-GBCA application are shown again, as illustrated in Figure S6, http://links.lww.com/RLI/B105. Mean T_1 relaxation times measured *in vivo* 10 days post-GBCA *in vivo* administration deviate only slightly from calibrated values inside the brain regions medulla (Fig. 7A) and the cerebellar cortex (Fig. 7B) for both EAE and HC mice and both GBCA. Inside the CN, the same holds true for both EAE and HC mice but only after gadobutrol treatment (Fig. 7C). In contrast, a strong negative T_1 deviation (Fig. 7C) was observed after gadopentetate treatment, that is, the T_1 relaxation times measured *in vivo* post-GBCA administration were longer than the corresponding *in vitro* calibrated T_1 (see Supplemental Digital Content 3, http://links.lww.com/RLI/B105 for further explanation). Thus, the retained Gd inside the CN 10 days after repeated gadopentetate administration lowers T_1 in *in vivo* MRI less than expected for the LA-ICP-MS-determined concentration. This effect was about 1.5-fold stronger in EAE compared with HC mice (mean ± SD; EAE vs. HC; CN: –22.4 ± 8.3% vs. –14.8 ± 3.1%). The relaxation time deviation is consistent with either a markedly reduced relaxivity $r_{1,eff}$ (EAE vs HC; CN: 1.45 $s^{-1}mM^{-1}$ vs 0.78 $s^{-1}mM^{-1}$) compared with the *in vitro* result in homogenized brain tissue ($r_{1,eff}$ = 4.35 $s^{-1}mM^{-1}$), or with a severely reduced effective average Gd concentration $C_{Gd,eff}$ (EAE vs HC; CN: 14.4 μM vs 3.7 μM)

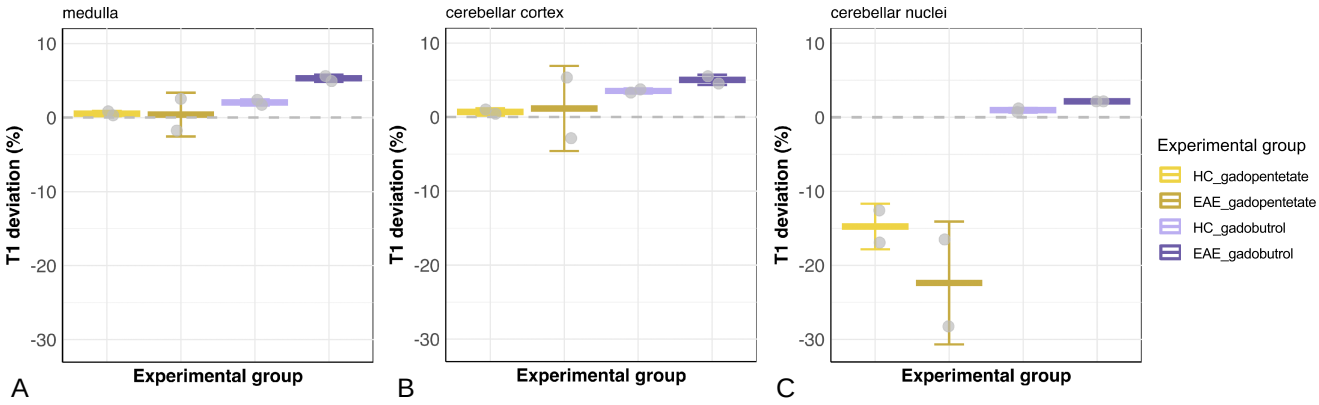

FIGURE 7. The mean T_1 deviation (%) 10 days post-GBCA administration is displayed for (A) the medulla, (B) the cerebellar cortex, and (C) the CN for both tested GBCAs. Data are displayed for n = 2 mice per experimental group, based on regional Gd concentrations quantified by LA-ICP-MS within the experimental framework previously described.[48] The crossbars represent the mean, and whiskers indicate ±1 SD. Within the CN area, *in vivo* T_1 values after gadopentetate administration deviated negatively from calibrated values. However, low sample sizes (n = 2/group, respectively) did not allow for statistical group comparisons.

compared with the absolute LA-ICP-MS-detected Gd concentrations[48] C_{Gd} (: mean ± SD; EAE vs. HC; CN: 42.60 ± 10.57 μM vs. 21.28 ± 3.72 μM; also see Table S3, Supplemental Digital Content 3, http://links.lww.com/RLI/B105 for full results).

DISCUSSION

In biopsies from gadopentetate-treated mice, cw EPR spectra revealed that roughly 70% correspond to intact GBCA complexes and the rest to Gd^{3+} in a different environment, resulting in magnetic parameters similar to those in aqueous solution. The occurrence of Gd^{3+} outside the GBCA complex supports the assumption that, in our EAE inflammation model, at least part of the administered Gd was released *in vivo* from the chelate, which is more likely from the kinetically less stable linear GBCAs.[23,29,30,48] However, cw EPR is inconclusive with respect to a possible Gd^{3+} release from gadobutrol, since the pure gadobutrol spectrum and the $GdCl_3$ (Gd^{3+}) reference spectrum are too similar for a distinction. Therefore, ^{1}H ENDOR was performed, which allows to test with high resolution for changes in the immediate environment of the Gd^{3+} (also see Supplemental Digital Content 4 Fig. S7, http://links.lww.com/RLI/B106). ENDOR spectroscopy revealed that in the case of gadobutrol, the ligand structure is retained, providing evidence for retention of intact gadobutrol. For gadopentetate, ENDOR confirmed the partial release of Gd^{3+} from the pentetate ligand, as concluded from cw EPR.

In addition, we detected 2 clear discrepancies between the EPR and LA-ICP-MS data. First, the concentration range determined by LA-ICP-MS in case of the linear gadopentetate is significantly larger than that from EPR, and second, LA-ICP-MS shows a strong difference between CN[48] and cerebellar cortex as well as medulla, while EPR detects similar concentrations. The latter goes in parallel with the findings from the calibrated *in vivo* MRI. This aspect will be discussed in more detail below.

In the *ex vivo* study on organotypic hippocampal slices, the concentration of Gd retained after incubation with both GBCAs lies between 8 and 10 μM, corresponding to about 0.8% to 1% of the originally administered GBCA dose. Considering the reported concentration detected by ICP-MS in postmortem human brain tissue,[20,52,70] the Gd concentrations within hippocampal slices after incubation with 1 mM GBCA can be considered clinically relevant. However, no evidence for Gd^{3+} release was found in the slices, since the spectra for both utilized GBCAs were highly similar to the pure GBCA spectra.

It is known that Gd^{3+} has a high affinity to phosphates with a solubility product of around 10^{-25},[71] and phosphorus close to Gd accumulation was reported in different studies.[25,72,73] A high binding affinity of ATP to Gd^{3+} has been shown and direct Gd complexation by ATP occurs in ATP/gadopentetate mixtures, while a ternary DTPA-ATP complex has been excluded.[74] Using P ENDOR, we demonstrated here the presence of phosphate in the immediate Gd environment in the biopsy sample as well as in the ATP/gadopentetate mixture. Contributions from Mn^{2+}-P hyperfine couplings could be excluded (see Supplemental Digital Content 5, Fig. S8, http://links.lww.com/RLI/B107). The Gd-P distance of 0.35 ± 0.01 nm in the gadopentetate-treated EAE biopsy is slightly smaller than the 0.36 ± 0.01 nm for Gd-ATP and in the ATP/gadopentetate mixture. Due to the slightly smaller Gd-P distance seen in the biopsy sample than for Gd-ATP we tentatively exclude a transchelation from the GBCA to ATP. An additional reference ENDOR experiment was performed on Gd-DMPC, since lanthanides have been shown to bind to phospholipids[75,76] and DMPC is an abundant phospholipid in mouse brain tissue.[77] Again, a Gd-P distance of 0.36 nm was found, but with a much lower SNR of the spectrum and concomitantly larger error margin of ±0.03 nm. The limited SNR of the DMPC-Gd reference P ENDOR spectrum precludes any conclusion on the involvement of the phospholipid in Gd transchelation.

The splitting in the P ENDOR measurements of the chronic brain slices incubated with both GBCA is visibly smaller and corresponds to a Gd-P distance of 0.37 ± 0.01 nm. From cw EPR and ^{1}H ENDOR measurements, we concluded that both GBCA retained in slices stayed intact. Therefore, it was surprising to see P atoms in such a vicinity to Gd. A possible explanation is that a phosphate group might occupy the water exchange site of the GBCA. ATP can be excluded as a binding partner since a gadobutrol-ATP reference sample yielded no detectable P ENDOR spectrum. Possible candidates would again be phospholipids[75,76] as well as proteins or sugars with

phosphorylated residues, including components of the ECM.[78,79]

The biopsy sample of the gadobutrol-treated EAE mouse, which also contained only intact GBCA as determined by ^{1}H ENDOR, showed no P in the close vicinity of Gd. This observation suggests that GBCA applied directly to the surface of tissue slices is retained differently than GBCA administered intravenously *in vivo* and subsequently detected in biopsies. *In vivo*, the contrast agents reach the tissue only after interacting with physiological transport and barrier structures and molecules, such as serum proteins[33,36] or vasculature-associated cellular and ECM components.[28,34,36,37,80]

In vitro MRI calibration on homogenized brain tissue spiked with Gd revealed that the T_1 relaxation time observed by *in vivo* MRI post-gadopentetate administration was significantly longer than expected for the Gd concentration as detected by LA-ICP-MS.[48] However, post-gadobutrol administration, the T_1 shortening effect reflected well the LA-ICP-MS expectations in both EAE and HC brains. Similar discrepancies between conventional T_1-weighted MRI[27] or quantitative $T1$-mapping-based measures[48,59] and elemental Gd quantification have been reported. On the basis of our observed difference between the linear and macrocyclic GBCA, we suggest that these inconsistencies may, at least in part, arise from the formation of relaxation-inactive Gd species following administration of kinetically less stable linear GBCAs, particularly in the context of neuroinflammation. This is consistent with previous findings showing that a substantial portion of retained Gd in rat brain occurs as phosphate-associated deposits, mainly composed of $GdPO_4$.[25,33] Such inorganic $GdPO_4$ salt deposits likely arise due to their low solubility, which is a possible reason for a weak relaxivity in MRI and loss of EPR signal. No substantial Gd^{3+} release and thereby no inorganic deposits seem to occur for gadobutrol. Reduced relaxometric visibility may also result from sequestration of Gd species within cellular compartments characterized by restricted water exchange, as suggested by Furlan et al.[49] However, with currently available MRI techniques, a direct differentiation between intra- and extracellular Gd species is not feasible. Moreover, in EAE, the formation of insoluble precipitates after IV gadopentetate injection may be additionally promoted by inflammation-related changes in endogenous ion homeostasis (eg, zinc) and reduced chelate stability.[48,81] In this line, after linear GBCA administration in humans or rodents, insoluble sea-urchin-shaped deposits were found in CN specimens, within capillary walls[29,49,52] or neuronal nuclei.[49,50] The CN contains a high density of neuronal bodies that are metabolically active, potentially leading to accumulation of inorganic phosphates.

While such inorganic deposits are invisible to EPR, it does detect retained Gd that either remained in the intact GBCA complex or is bound to alternative complexing species. Binding of released Gd^{3+} to macromolecular moieties might be a reason for differences in the relaxation-effective Gd concentration as determined by calibrated MRI and the EPR-visible Gd concentration. The relaxivity of Gd^{3+} bound to macromolecules can be significantly higher than for GBCA complexes.[82,83] A relaxivity enhancement by a factor of 5 was previously observed by others.[84] Such increased relaxivity of the 30% fraction of Gd found outside the GBCA would lead to an overestimation of the relaxation-active Gd concentration by more than a factor of 2 and thereby significantly underestimate the amount of Gd in inorganic deposits. However, this would still only explain part of the Gd missing in EPR and requires further exploration.

Limitations of the Study

The EAE mouse model reiterates the main neuropathological hallmarks of MS, but may not fully reflect the spectrum of disease heterogeneity in humans.[85] In addition, the experimental design, including frequency and daily GBCA doses, differed significantly from applications in clinical practice. However, for consistency, the chosen treatment regimen adhered to our previous publications.[47,48] The low sample size included in the study precluded quantitative statistical analysis.

Although organotypic brain slice cultures maintain tissue integrity, including vessels,[86] and responsiveness to inflammatory stimuli,[87] the variations in mouse strains, GBCA doses, and tissue preparation methods as well as the obvious exclusion of blood-brain barrier-related effects complicated direct comparisons between *ex* and *in vivo* samples. Moreover, a successful chronic slice culture was not feasible without the use of P-containing buffer (PBS), which in turn could affect our findings on Gd^{3+} release and binding.

Quantification of Gd with cw EPR as well as LA-ICP-MS is based on relative comparisons to known standards, which could introduce additional deviations. Currently, no certified reference materials are available for LA-ICP-MS and we can only rely on homemade matrix-matched standards for calibration. The amount of EPR-active Gd in the tissue samples is partially close to our current detection limit, yielding spectra with low SNR. In addition, the accuracy of the EPR quantification could be affected by uncertainties in the exact sample volume within the EPR tube, even though this problem is in part eliminated by the normalization on the Mn content. Unlike LA-ICP-MS, which utilizes thin tissue sections with precise spatial resolution,[48] our EPR analyses were conducted on biopsied tissues, which inherently possess lower spatial precision and may result in admixture with brain regions exhibiting lower Gd retention. Due to the limited amount of remaining tissue available for EPR biopsies, comparative parallel destructive elemental analysis of the same samples by bulk ICP-MS was not feasible.

Regarding ENDOR measurements, it is possible that not all Gd-P couplings were detected, as the first delay ($\tau = 470$ ns) in ^{31}P Mims ENDOR was optimized based on the Gd-ATP sample, therefore potentially overlooking stronger Gd-P couplings in mouse biopsy samples.

CONCLUSIONS

In summary, we have shown that *in vivo* Gd retention after GBCA applications can be detected by cw EPR and pulsed ENDOR on cerebellar cortex biopsy samples as well as chronic organotypic hippocampal tissue slices, both of sub-mm dimensions. Thereby, we successfully separated the Gd signal from the significantly stronger Mn^{2+} signal, a common challenge in EPR measurements on biological samples. In all EAE biopsies, the Gd retention range was about 2 to 3 μM as determined by cw EPR, regardless of the GBCA used. In the HC cerebellar samples, the Gd amount was significantly lower after gadopentetate application, and no Gd was detectable after gadobutrol application, confirming previous findings on inflammation-promoted Gd retention. Gd^{3+} release was detected only from the linear gadopentetate in biopsy samples but not in organotypic brain slices, where both gadopentetate and gadobutrol remained intact, confirming previous reports.[48,49]

Interestingly, ENDOR measurements revealed a chelation of the released Gd^{3+} in the cerebellar biopsy by phosphate-containing moieties. Phosphate was also found in the surrounding of the intact gadopentetate and gadobutrol in the

tissue slices. These findings underscore the complexity of GBCA interactions in brain tissue and highlight the importance of integrating *in vivo* and *ex vivo* approaches to elucidate the mechanisms underlying sustained Gd retention. Notably, 1 to 10 μM Gd retention has been reported in human tissue after multiple GBCA administrations[51] and in the 1 μM range in human brain tissue even after single GBCA administration.[88] Thus, the detection of retained Gd and the distinction between intact GBCA and released species on the biopsy level by EPR/ENDOR opens new routes for organ- and tissue-specific human studies.

Lastly, our MRI *in vitro* calibration experiments suggest that a substantial portion of retained Gd within the CN may be undetected by *in vivo* MRI after repeated gadopentetate administration, particularly in the context of neuroinflammation. While MRI remains one of the best diagnostic tools for brain pathologies in clinical practice, the potential underestimation of the true extent of long-lasting Gd retention in specific brain regions is of considerable clinical importance, particularly for patients with neuroinflammatory conditions.

REFERENCES

1. Runge VM. Dechelation (transmetalation): consequences and safety concerns with the linear gadolinium-based contrast agents, in view of recent health care rulings by the EMA (Europe), FDA (United States), and PMDA (Japan). *Invest Radiol*. 2018;53:571–578.
2. Hao D, Ai T, Goerner F, et al. MRI contrast agents: basic chemistry and safety. *J Magn Reson Imaging*. 2012;36:1060–1071.
3. Kanda T, Ishii K, Kawaguchi H, et al. High signal intensity in the dentate nucleus and globus pallidus on unenhanced T1-weighted MR images: relationship with increasing cumulative dose of a gadolinium-based contrast material. *Radiology*. 2014;270:834–841.
4. Errante Y, Cirimele V, Mallio CA, et al. Progressive increase of T1 signal intensity of the dentate nucleus on unenhanced magnetic resonance images is associated with cumulative doses of intravenously administered gadodiamide in patients with normal renal function, suggesting dechelation. *Invest Radiol*. 2014;49:685–690.
5. Quattrocchi CC, Mallio CA, Errante Y, et al. Gadodiamide and dentate nucleus T1 hyperintensity in patients with meningioma evaluated by multiple follow-up contrast-enhanced magnetic resonance examinations with no systemic interval therapy. *Invest Radiol*. 2015;50:470–472.
6. Weberling LD, Kieslich PJ, Kickingereder P, et al. Increased signal intensity in the dentate nucleus on unenhanced T1-weighted images after gadobenate dimeglumine administration. *Invest Radiol*. 2015;50:743–748.
7. Ramalho J, Castillo M, AlObaidy M, et al. High signal intensity in globus pallidus and dentate nucleus on unenhanced T1-weighted MR images: evaluation of two linear gadolinium-based contrast agents. *Radiology*. 2015;276:836–844.
8. Kanda T, Osawa M, Oba H, et al. High signal intensity in dentate nucleus on unenhanced T1-weighted MR Images: association with linear versus macrocyclic gadolinium chelate administration. *Radiology*. 2015;275:803–809.
9. Robert P, Lehericy S, Grand S, et al. T1-weighted hypersignal in the deep cerebellar nuclei after repeated administrations of gadolinium-based contrast agents in healthy rats: difference between linear and macrocyclic agents. *Invest Radiol*. 2015;50:473–480.
10. Robert P, Violas X, Grand S, et al. Linear gadolinium-based contrast agents are associated with brain gadolinium retention in healthy rats. *Invest Radiol*. 2016;51:73–82.
11. Frenzel T, Apte C, Jost G, et al. Quantification and assessment of the chemical form of residual gadolinium in the brain after repeated administration of gadolinium-based contrast agents: comparative study in rats. *Invest Radiol*. 2017;52:396–404.
12. Lohrke J, Frisk AL, Frenzel T, et al. Histology and gadolinium distribution in the rodent brain after the administration of cumulative high doses of linear and macrocyclic gadolinium-based contrast agents. *Invest Radiol*. 2017;52:324–333.
13. Jost G, Frenzel T, Boyken J, et al. Long-term excretion of gadolinium-based contrast agents: linear versus macrocyclic agents in an experimental rat model. *Radiology*. 2019;290:340–348.
14. Davies J, Marino M, Smith APL, et al. Repeat and single dose administration of gadodiamide to rats to investigate concentration and location of gadolinium and the cell ultrastructure. *Sci Rep*. 2021;11:13950.
15. Bussi S, Coppo A, Botteron C, et al. Differences in gadolinium retention after repeated injections of macrocyclic MR contrast agents to rats. *J Magn Reson Imaging*. 2018;47:746–752.
16. Bussi S, Coppo A, Celeste R, et al. Macrocyclic MR contrast agents: evaluation of multiple-organ gadolinium retention in healthy rats. *Insights Imaging*. 2020;11:11.
17. Frenzel T, Ulbrich HF, Pietsch H. The macrocyclic gadolinium-based contrast agents gadobutrol and gadoteridol show similar elimination kinetics from the brain after repeated intravenous injections in rabbits. *Invest Radiol*. 2021;56:341–347.
18. Strzeminska I, Factor C, Robert P, et al. Long-term evaluation of gadolinium retention in rat brain after single injection of a clinically relevant dose of gadolinium-based contrast agents. *Invest Radiol*. 2020;55:138–143.
19. Radbruch A, Haase R, Kieslich PJ, et al. No signal intensity increase in the dentate nucleus on unenhanced T1-weighted MR images after more than 20 serial injections of macrocyclic gadolinium-based contrast agents. *Radiology*. 2017;282:699–707.
20. Murata N, Murata K, Gonzalez-Cuyar LF, et al. Gadolinium tissue deposition in brain and bone. *Magn Reson Imaging*. 2016;34:1359–1365.
21. European Medicines Agency. EMA's final opinion confirms restrictions on use of linear gadolinium agents in body scan. July 21, 2017. Assessed July 12, 2025 https://www.ema.europa.eu/en/news/emas-final-opinion-confirms-restrictions-use-linear-gadolinium-agents-body-scans
22. U.S. Food and Drug Administration. FDA warns that gadolinium-based contrast agents (GBCAs) are re-tained in the body; requires new class warnings. December 19, 2017. Accessed July 12, 2025 https://www.fda.gov/drugs/fda-drug-safety-podcasts/fda-drug-safety-podcast-fda-warns-gadolinium-based-contrast-agents-gbcas-are-retained-body-requires
23. Frenzel T, Lengsfeld P, Schirmer H, et al. Stability of gadolinium-based magnetic resonance imaging contrast agents in human serum at 37 degrees C. *Invest Radiol*. 2008;43:817–828.
24. Port M, Idee JM, Medina C, et al. Efficiency, thermodynamic and kinetic stability of marketed gadolinium chelates and their possible clinical consequences: a critical review. *BioMetals*. 2008;21:469–490.
25. Strzeminska I, Factor C, Jimenez-Lamana J, et al. Comprehensive speciation analysis of residual gadolinium in deep cerebellar nuclei in rats repeatedly administered with gadoterate meglumine or gadodiamide. *Invest Radiol*. 2022;57:283–292.
26. Strzeminska I, Factor C, Robert P, et al. Speciation analysis of gadolinium in the water-insoluble rat brain fraction after administration of gadolinium-based contrast agents. *Invest Radiol*. 2021;56:535–544.
27. Robert P, Fingerhut S, Factor C, et al. One-year retention of gadolinium in the brain: comparison of gadodiamide and gadoterate meglumine in a rodent model. *Radiology*. 2018;288:424–433.
28. Gianolio E, Bardini P, Arena F, et al. Gadolinium retention in the rat brain: assessment of the amounts of insoluble gadolinium-containing species and intact gadolinium complexes after repeated administration of gadolinium-based contrast agents. *Radiology*. 2017;285:839–849.
29. Fingerhut S, Sperling M, Holling M, et al. Gadolinium-based contrast agents induce gadolinium deposits in cerebral vessel walls, while the neuropil is not affected: an autopsy study. *Acta Neuropathol*. 2018;136:127–138.
30. Rasschaert M, Emerit A, Fretellier N, et al. Gadolinium retention, brain T1 hyperintensity, and endogenous metals: a comparative study of macrocyclic versus linear gadolinium chelates in renally sensitized rats. *Invest Radiol*. 2018;53:328–337.
31. Thakral C, Abraham JL. Gadolinium-induced nephrogenic systemic fibrosis is associated with insoluble Gd deposits in tissues: in vivo transmetallation confirmed by microanalysis. *J Cutan Pathol*. 2009;36:1244–1254.
32. Telgmann L, Wehe CA, Kunnemeyer J, et al. Speciation of Gd-based MRI contrast agents and potential products of transmetalation with iron ions or parenteral iron supplements. *Anal Bioanal Chem*. 2012;404:2133–2141.

33. Rasschaert M, Weller RO, Schroeder JA, et al. Retention of gadolinium in brain parenchyma: pathways for speciation, access, and distribution. A critical review. *J Magn Reson Imaging*. 2020;52:1293–1305.
34. Werner P, Taupitz M, Schroder L, et al. An NMR relaxometry approach for quantitative investigation of the transchelation of gadolinium ions from GBCAs to a competing macromolecular chelator. *Sci Rep*. 2021;11: 21731.
35. Vander Elst L, Muller RN. A 31P and 1H NMR relaxometric study of the interaction between adenosine triphosphate (ATP) and paramagnetic ions (Gd3+ and Mn2+). *Inorganica Chim Acta*. 1998;273: 92–100.
36. Werner P, Schuenke P, Krylova O, et al. Investigating the role of sulfate groups for the binding of Gd(3+) ions to glycosaminoglycans with NMR relaxometry. *ChemMedChem*. 2022;17:e202100764.
37. Taupitz M, Stolzenburg N, Ebert M, et al. Gadolinium-containing magnetic resonance contrast media: investigation on the possible transchelation of Gd^{3+} to the glycosaminoglycan heparin. *Contrast Media Mol Imaging*. 2013;8:108–116.
38. Roccatagliata L, Vuolo L, Bonzano L, et al. Multiple sclerosis: hyperintense dentate nucleus on unenhanced T1-weighted MR images is associated with the secondary progressive subtype. *Radiology*. 2009; 251:503–510.
39. Schlemm L, Chien C, Bellmann-Strobl J, et al. Gadopentetate but not gadobutrol accumulates in the dentate nucleus of multiple sclerosis patients. *Mult Scler*. 2017;23:963–972.
40. Malhotra A, LeSar B, Wu X, et al. Progressive T1 shortening of the dentate nucleus in patients with multiple sclerosis: result of multiple administrations of linear gadolinium contrast agents versus intrinsic disease. *AJR Am J Roentgenol*. 2018;211:1099–1105.
41. Kang H, Hii M, Le M, et al. Gadolinium deposition in deep brain structures: relationship with dose and ionization of linear gadolinium-based contrast agents. *AJNR. Am J Neuroradiol*. 2018;39:1597–1603.
42. Eisele P, Szabo K, Ebert A, et al. Diffusion-weighted imaging of the dentate nucleus after repeated application of gadolinium-based contrast agents in multiple sclerosis. *Magn Reson Imaging*. 2019;58:1–5.
43. Stojanov DA, Aracki-Trenkic A, Vojinovic S, et al. Increasing signal intensity within the dentate nucleus and globus pallidus on unenhanced T1W magnetic resonance images in patients with relapsing-remitting multiple sclerosis: correlation with cumulative dose of a macrocyclic gadolinium-based contrast agent, gadobutrol. *Eur Radiol*. 2016;26: 807–815.
44. Splendiani A, Perri M, Marsecano C, et al. Effects of serial macrocyclic-based contrast materials gadoterate meglumine and gadobutrol administrations on gadolinium-related dentate nuclei signal increases in unenhanced T1-weighted brain: a retrospective study in 158 multiple sclerosis (MS) patients. *Radiol Med*. 2018;123:125–134.
45. Agris J, Pietsch H, Balzer T. What evidence is there that gadobutrol causes increasing signal intensity within the dentate nucleus and globus pallidus on unenhanced T1W MRI in patients with RRMS? *Eur Radiol*. 2016;26:816–817.
46. Jaulent P, Hannoun S, Kocevar G, et al. Weekly enhanced T1-weighted MRI with Gadobutrol injections in MS patients: is there a signal intensity increase in the dentate nucleus and the globus pallidus? *Eur J Radiol*. 2018;105:204–208.
47. Wang S, Hesse B, Roman M, et al. Increased retention of gadolinium in the inflamed brain after repeated administration of gadopentetate dimeglumine: a proof-of-concept study in mice combining ICP-MS and Micro- and nano-SR-XRF. *Invest Radiol*. 2019;54:617–626.
48. Anderhalten L, Silva RV, Morr A, et al. Different impact of gadopentetate and gadobutrol on inflammation-promoted retention and toxicity of gadolinium within the mouse brain. *Invest Radiol*. 2022; 57:677–688.
49. Furlan C, Montarolo F, Di Gregorio E, et al. Analysis of the gadolinium retention in the experimental autoimmune encephalomyelitis (EAE) murine model of multiple sclerosis. *J Trace Elem Med Biol*. 2021;68: 126831.
50. McDonald RJ, McDonald JS, Kallmes DF, et al. Gadolinium deposition in human brain tissues after contrast-enhanced MR imaging in adult patients without intracranial abnormalities. *Radiology*. 2017;285: 546–554.
51. Roberts DR, Welsh CA, LeBel DP 2nd, et al. Distribution map of gadolinium deposition within the cerebellum following GBCA administration. *Neurology*. 2017;88:1206–1208.
52. McDonald RJ, McDonald JS, Kallmes DF, et al. Intracranial gadolinium deposition after contrast-enhanced MR imaging. *Radiology*. 2015;275:772–782.
53. Okabayashi S, Kawane L, Mrabawani NY, et al. Speciation analysis of gadolinium-based contrast agents using aqueous eluent-hydrophilic interaction liquid chromatography hyphenated with inductively coupled plasma-mass spectrometry. *Talanta*. 2021;222:121531.
54. Le Fur M, Caravan P. The biological fate of gadolinium-based MRI contrast agents: a call to action for bioinorganic chemists. *Metallomics*. 2019;11:240–254.
55. Le Fur M, Moon BF, Zhou IY, et al. Gadolinium-based contrast agent biodistribution and speciation in rats. *Radiology*. 2023;309:e230984.
56. Goldfarb D. Exploring protein conformations in vitro and in cell with EPR distance measurements. *Curr Opin Struct Biol*. 2022;75:102398.
57. Bonucci A, Ouari O, Guigliarelli B, et al. In-cell EPR: progress towards structural studies inside cells. *Chembiochem*. 2020;21:451–460.
58. Ludwig R, Malla B, Hohrhan M, et al. Investigating the mitoprotective effects of S1P receptor modulators ex vivo using a novel semi-automated live imaging set-up. *Int J Mol Sci*. 2023;25:261.
59. Hua N, Minaeva O, Lupoli N, et al. Gadolinium deposition in the rat brain measured with quantitative MRI versus elemental mass spectrometry. *Radiology*. 2023;306:244–251.
60. Wang Q, Andreasson K. The organotypic hippocampal slice culture model for examining neuronal injury. *J Vis Exp*. 2010;44:e2106.
61. Raitsimring AM, Astashkin AV, Poluektov OG, et al. High-field pulsed EPR and ENDOR of Gd3+ complexes in glassy solutions. *Appl Magn Reson*. 2005;28:281–295.
62. Hofbauer W, Bittl R. A novel approach to separating EPR lines arising from species with different transition moments. *J Magn Reson*. 2000;147: 226–231.
63. Mims WB. Pulsed endor experiments. *Proc R Soc Lond*. 1965;A283: 452–457.
64. The MathWorks, Inc. MATLAB version: 9.14.0.2206163 (R2023a). 2023. https://www.mathworks.com
65. Stoll S, Schweiger A. EasySpin, a comprehensive software package for spectral simulation and analysis in EPR. *J Magn Reson*. 2006;178:42–55.
66. Pintaske J, Martirosian P, Graf H, et al. Relaxivity of gadopentetate dimeglumine (Magnevist), gadobutrol (Gadovist), and gadobenate dimeglumine (MultiHance) in human blood plasma at 0.2, 1.5, and 3 Tesla. *Invest Radiol*. 2006;41:213–221.
67. Palagi L, Longo DL, Toth E, et al. Molecular and supramolecular routes to enhance Gadolinium-based contrast agents relaxivity: how far are we from the theoretical optimal value? *Eur J Med Chem*. 2025;292:117668.
68. Pyle HK, Judd M, Barancewicz A, et al. Elucidating polyphosphate anion binding to lanthanide complexes using EXAFS and pulsed EPR spectroscopy. *Inorg Chem*. 2024;63:20726–20736.
69. Litvinov A, Feintuch A, Un S, et al. Triple resonance EPR spectroscopy determines the Mn(2+) coordination to ATP. *J Magn Reson*. 2018;294: 143–152.
70. Kanda T, Fukusato T, Matsuda M, et al. Gadolinium-based contrast agent accumulates in the brain even in subjects without severe renal dysfunction: evaluation of autopsy brain specimens with inductively coupled plasma mass spectroscopy. *Radiology*. 2015;276:228–232.
71. Firsching FH, Brune SN. Solubility products of the trivalent rare-earth phosphates. *J Chem Eng Data*. 1991;36:93–95.
72. Sieber MA, Lengsfeld P, Frenzel T, et al. Preclinical investigation to compare different gadolinium-based contrast agents regarding their propensity to release gadolinium in vivo and to trigger nephrogenic systemic fibrosis-like lesions. *Eur Radiol*. 2008;18:2164–2173.
73. George SJ, Webb SM, Abraham JL, et al. Synchrotron X-ray analyses demonstrate phosphate-bound gadolinium in skin in nephrogenic systemic fibrosis. *Br J Dermatol*. 2010;163:1077–1081.
74. Elst L, Van Haverbeke Y, Goudemant JF, et al. Stability assessment of gadolinium complexes by P-31 and H-1 relaxometry. *Magn Reson Med*. 1994;31:437–444.
75. Evans CH. *Biochemistry of the Lanthanides*. Boston, MA: Springer US; 1990.

76. Unruh C, Van Bavel N, Anikovskiy M, et al. Benefits and detriments of gadolinium from medical advances to health and ecological risks. *Molecules*. 2020;25:5762.
77. Fitzner D, Bader JM, Penkert H, et al. Cell-type- and brain-region-resolved mouse brain lipidome. *Cell Rep*. 2020;32:108132.
78. Yalak G, Olsen BR. Proteomic database mining opens up avenues utilizing extracellular protein phosphorylation for novel therapeutic applications. *J Transl Med*. 2015;13:125.
79. Bailey S, Sroga GE, Hoac B, et al. The role of extracellular matrix phosphorylation on energy dissipation in bone. *eLife*. 2020;9:e58184.
80. Habermeyer J, Boyken J, Harrer J, et al. Comprehensive phenotyping revealed transient startle response reduction and histopathological gadolinium localization to perineuronal nets after gadodiamide administration in rats. *Sci Rep*. 2020;10:22385.
81. Tweedle MF, Wedeking P, Kumar K. Biodistribution of radiolabeled, formulated gadopentetate, gadoteridol, gadoterate, and gadodiamide in mice and rats. *Invest Radiol*. 1995;30:372–380.
82. Rohrer M, Bauer H, Mintorovitch J, et al. Comparison of magnetic properties of MRI contrast media solutions at different magnetic field strengths. *Invest Radiol*. 2005;40:715–724.
83. Lohrke J, Frenzel T, Endrikat J, et al. 25 years of contrast-enhanced MRI: developments, current challenges and future perspectives. *Adv Ther*. 2016;33:1–28.
84. Berki TR, Martinelli J, Tei L, et al. Polymerizable Gd(iii) building blocks for the synthesis of high relaxivity macromolecular MRI contrast agents. *Chem Sci*. 2021;12:3999–4013.
85. Procaccini C, De Rosa V, Pucino V, et al. Animal models of multiple sclerosis. *Eur J Pharmacol*. 2015;759:182–191.
86. Humpel C. Organotypic brain slice cultures. *Curr Protoc Immunol*. 2018;123:e59.
87. Huuskonen J, Suuronen T, Miettinen R, et al. A refined in vitro model to study inflammatory responses in organotypic membrane culture of postnatal rat hippocampal slices. *J Neuroinflammation*. 2005;2:25.
88. Kobayashi M, Levendovszky SR, Hippe DS, et al. Comparison of human tissue gadolinium retention and elimination between gadoteridol and gadobenate. *Radiology*. 2021;300:559–569.

